A metaporoelastic structure that overcomes the sound insulation weaknesses of single and double panel partitions

Ke Li, Nicolas Dauchez, Benoit Nennig

Version of Record: https://www.sciencedirect.com/science/article/pii/S0003682X23002074
Manuscript_cd400a0757f6f40a9c49efebfab16277

A metaporoelastic structure that overcomes the sound insulation weaknesses of single and double panel partitions

Ke Li[a], Nicolas Dauchez[a,*], Benoit Nennig[b]

[a] *Université de technologie de Compiègne, Alliance Sorbonne Université, Laboratoire Roberval, Centre de recherche Royallieu, CS 60319, 60203 Compiègne Cedex, France*
[b] *Institut supérieur de mécanique de Paris (ISAE-SUPMECA), Laboratoire Quartz EA 7393, 3 rue Fernand Hainaut, 93407 Saint-Ouen sur Seine, France.*

Abstract

Single and double panel partitions are well known for their sound transmission loss weaknesses in the vicinity of their structural resonances: the first mode of the finite size panel and the mass-spring-mass resonance of the double panel. In this paper, we investigate the use of a poroelastic based metamaterial to address this problem. The metamaterial is a network of poroelastic beams, the first bending mode of which is tuned at the targeted panel resonance. The porous nature of the resonators allows taking advantage of its dissipative properties stemming from the interaction between solid and fluid phases. For the double panel application, where a porous layer is generally present, the effectiveness of the poroelastic metamaterial relies on the design of its shape and mounting conditions. First, the sound transmission loss of a finite size single panel is studied experimentally in a rectangular duct under normal incidence. It is shown that the poroelastic metamaterial increases the transmission loss up to 12 dB at the first mode of the panel. Using resonators tuned at different frequencies makes it possible to spread this gain. The attenuation mechanisms are analyzed by simulation using a finite element model. Secondly, the double panel partition is investigated with a periodic finite element model using the Floquet-Bloch theorem. Finally, the impact of several parameters like airflow resistivity and filling fraction on the efficiency of the metaporoelastic structure is illustrated considering a diffuse field excitation.

Keywords: Finite size single panel, Double panel partition, Poroelastic material, Sound insulation, Transmission loss, Acoustic metamaterial, Thermocompressed melamine foam, Periodic resonators, Metaporoelastic structure

1. Introduction

To save energy and resources during manufacturing and life cycle, compact and lightweight structures are increasingly sought, especially in the construction and transport sectors. However, the acoustic insulation of an infinite single panel is mainly driven by the *mass law*, which states the heavier the better. When dealing with finite size panels [1], the first resonance of the structure induces a severe dip in its sound insulation. Similar behavior is also observed on curved panels, close to the ring frequency [2, 3]. Below this frequency, the transmission loss (TL) is controlled by the panel stiffness and decreases by 6 dB per octave. Close to the resonances, the TL is minimal and controlled by damping. Above the first resonance frequency, TL tends to obey mass law up to the coincidence frequency [1]. The coincidence phenomenon occurs when the projection of the incident acoustic wavenumber is equal to the free bending wavenumber in the panel, leading to poor sound insulation.

Double wall partitions are set up in practical applications to overcome the mass law: two panels are separated by an air gap, usually filled with a porous sound absorbing material [1]. This structure exhibits a mass-spring-mass resonance, beyond which the two panels are decoupled and outperform the single panel partition with the same mass.

*Corresponding author
Email address: nicolas.dauchez@utc.fr (Nicolas Dauchez)

However, close to this resonant frequency, the partition is nearly transparent. Fortunately, the inner porous layer reduces the consequences of air-gap acoustic resonances and helps to maintain efficient decoupling.

Another way to enhance the TL is to add resonators to change the effective mass [2, 4] of the panel or the effective stiffness of the core [5]. Such an approach has been recently modified and extended through the metamaterial paradigm, allowing better integrated solutions. Metamaterial and metasurfaces are designed with subwavelength resonators often arranged in periodic structures to control wave propagation and stop bands. Early works for sound insulation were based on bulk materials [6, 7] or Lamb waves, and rapidly spread to flexural wave manipulation in beams and plates [8–11]. In the meantime, metamaterials have been widely used in acoustics and especially to improve sound absorption [12, 13] (see the references therein).

Since sound attenuation by panels can present dips at localized frequencies, metamaterials are good candidates to overcome these limitations. Many works have proposed locally resonant metamaterials to enhance sound insulation of an infinite panel close to coincidence [14], to create stop bands [15], or tackle finite panel resonances or the ring frequency of curved panels [3]. For double panels, the mass-spring-mass resonance has been tackled by i) changing the core *effective dynamical stiffness* with Helmholtz resonators [5, 16, 17]; ii) changing the *effective dynamical mass*, without [18] and with a foam core [14, 16, 19–21]. The metamaterial's efficiency is mainly governed by the mass ratio between the resonators and the bare plate and by staggered tuning [22]. Generally, an added mass less than 10% can greatly enhance the TL. When subwavelength resonators are used, the effective parameters can be used in standard formulas [14, 18, 20] to simplify the design procedure.

Combining such an approach with porous or poroleastic materials [19–21] is of great interest since viscothermal losses improve sound absorption and impedance mismatch [21, 23], limiting the TL dips especially in a diffuse field. The practical implementation of passive resonators is performed with an array of cylindrical point masses [10], stepped resonators composed of a soft material with a heavy cap [15], a cantilever beam [22, 24], possibly 3D-printed systems [3, 18, 20], dual-beam resonators [25] or using the added mass and the elasticity of the foam core [19]. It is noteworthy that for a double panel, the resonator can be added inside the cavity [14, 19] to ensure compactness and robustness.

The aim of this paper is to investigate the potential offered by poroelastic resonators to improve the TL of a structure around two characteristic resonances: the first resonance of the finite size panel, and the mass-spring-mass resonance of the double panel. The resonators consist of poroelastic beams fixed to spaced supports, providing a simple and easy-to-manufacture solution. For double panels in particular, where a poroelastic layer is generally present, the solution simply consists of a specific implementation of the poroelastic layer: the approach proposed does not require any additional system. The native diphasic nature of the poroelastic resonator provides a natural way to combine the properties of the sound absorbing material and vibration control. Similar arrangements of poroelastic lamellas have proven their potential for sound absorption [26, 27] and attenuation in silencers [28]. The paper is organized as follows. First, the concept is described in its experimental implementation which addresses the first resonance of a single panel. It is mounted in a rectangular duct which allows the measurement of the sound transmission loss in normal incidence. This experimental configuration is then reproduced by finite element simulation to further analyze the interactions within the metaporoelastic structure. Finally, the double panel partition is investigated by simulation on the basis of a periodic finite element model. The role of several parameters involved in ensuring the efficiency of the metaporoelastic structure are shown.

2. Experimental implementation

In this section, we present an experimental implementation of the concept, applied to a finite size single panel. To obtain accurate measurements at low frequency, the TL is determined at normal incidence using a rectangular duct. This configuration provides good control of the first resonance of the host panel together with a frequency resolution adapted for observing resonant phenomena.

2.1. Test bench for transmission loss measurement

The test bench, shown in Fig. 1(a), is a rectangular duct of section 100 mm $\times$ 200 mm. It has been designed for acoustic multimodal characterization within the frequency band [100 Hz - 3.5 kHz], accounting for 10 propagative modes [29]. The multimodal scattering matrix, which contains the modal reflection and transmission coefficients of the first 10 acoustic propagating modes, is measured using a multi-source method described in reference [29] without

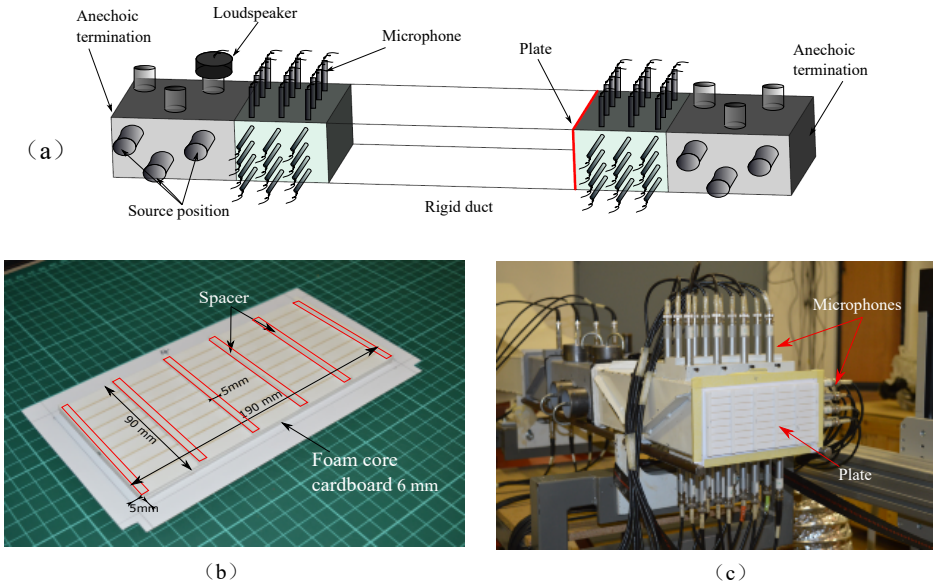

Figure 1: Experimental set-up. (a) Description of the multimodal test bench; (b) Plate without poroelastic beams; (3) Plate located on the measurement section before closing the duct.

flow. Using this method, we can obtain the amplitude of the incident and transmitted plane waves from which the transmission loss is determined. Since we are interested in the frequency range [100 Hz- 1.5 kHz], only 2 source positions are necessary because only 2 modes propagate below 1711 Hz: the plane wave mode and the mode (0,1) that propagates from 857 Hz. Broadband noise is chosen as the excitation signal and the measurements are repeated twice using three source positions to increase the measurement quality.

The panel tested (Fig. 1(b)) is clamped at the interface between a rigid wooden duct and the microphone section, as shown in Fig. 1(c).

2.2. Description of the single panel

The dimensions of the panel are chosen to fit in the test bench cross-section. A rather light structure has been chosen to keep a mass ratio of the poroelastic material over the panel of around 10%. Hence, the host structure is made of 2 juxtaposed plates of foam core cardboard each having a thickness of 3 mm and dimensions of 90 mm $\times$ 190 mm (see Fig. 1(b)). This structure is bonded on a soft and thin cardboard sheet of dimensions 126 mm $\times$ 226 mm clamped between two duct sections. In this manner, the distance between all the edges of the foam core cardboard plate and duct wall is 5 mm: this provides a reproducible boundary condition around the samples. The mass per unit area is 0.858 kg.m^{-2}. The first resonance of the elastic panel is around 300 Hz, as shown in Fig. 3.

2.3. Poroelastic metamaterial

The metamaterial is made up of an array of poroelastic beams fixed on several spaced supports (called spacers) added on the panel (see Fig. 2). This configuration will ensure a good coupling with the transverse motion of the panel. In order to control the first mode of the panel, the resonators have to be tuned around the same frequency.

Assuming an elastic behavior, an estimation of the first resonance frequencies of the clamped-clamped beam [30], are given by

$$f_i = \frac{\lambda_i^2}{2\pi\ell^2}\sqrt{\frac{EI}{\rho_1 S}}, \tag{1}$$

where $\lambda_1 \approx 4.73$, $\lambda_2 \approx 7.85$ and $\lambda_i \approx (2i+1)\frac{\pi}{2}$ for $i \geq 3$. E is the Young's modulus, ρ_1 is the density, $I = bH^3/12$ is the second moment of area, ℓ is the beam length, H is the beam thickness and $S = bH$ is the cross section area. To obtain a mass ratio of the metamaterial to the panel around 10% (see Tab. 3), we used thermocompressed melamine

Porosity ϕ	Airflow resistivity σ ($Nm^{-4}s$)	Viscous length Λ (μm)	Thermal length Λ' (μm)	Tortuosity α_∞	Density ρ_1 ($kg.m^{-3}$)	Young's modulus E (kPa)	Loss factor η	Poisson ratio ν
0.967	41 222	58	65	1.05	24.2	121.4	0.102	0.21

Table 1: Properties of the thermocompressed poroelastic material measured in the Roberval laboratory at UTC [32, 33].

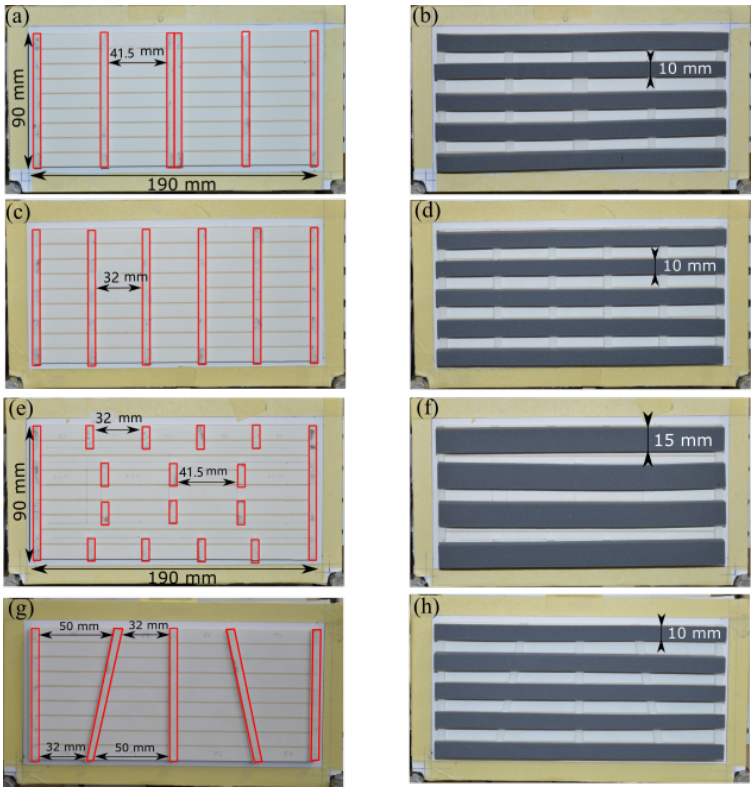

Figure 2: Arrangement of spacers (left) and resonators (right) on the panel for several configurations: P1(a-b), P2 (c-d), P3 (e-f), P4 (g-h).

foam with a compression rate of 2.9 [31, 32]. The mechanical and acoustical properties of this poroelastic material are listed in Tab. 1. They were determined by measurements carried out by the authors in the Roberval laboratory, as described in [32, 33].

The tuning of the resonant frequency can be done by changing ℓ. In this experiment, the poroelastic beams have the same length as the host structure, i.e., 190 mm, and are bonded on several rigid spacers made of 3 mm thick foam core cardboard, as shown in Fig. 2 (left side). The four resonators arrangements tested are depicted in Fig. 2 (right side). The thickness of each beam is $H = 10.4$ mm while the width b is either 10 mm or 15 mm.

The first two configurations depicted in Fig. 2(a-b, c-d), named P1 and P2, are designed to investigate the effect of beam length on TL. Five or six spacers are placed on the plate with the same periodicity, so that 20 beams of B1 type are used in the P1 configuration and 25 beams of B2 type are used in the P2 configuration. All the beams are fixed on the spacers with double-face tape.

Configurations P3 and P4 are designed to achieve a broadband effect by mixing resonators of various lengths. In the case of P3, the combination of eight beams of type B1 and ten beams of type B2 are used for the resonators, as illustrated in Fig. 2(e, f). Shorter spacers are used to produce this configuration and the width of the porous beam is 15 mm. For configuration P4 (see Fig. 2(g, h)), two spacers are located obliquely on the host plate to modify the length of the resonators. This achieves an equal distribution of type B1-5 poroelastic resonators on the plate surface. The distance between two poroelastic beams is 10 mm in all the configurations tested. The poroelastic beam network covers approximately 55% of the panel for configurations P1, P2 and P4 and 67% for arrangement P3.

	B1	B2	B3	B4	B5	mass ratio
Length of beam ℓ (mm)	41.5	32	36.5	45.5	50	
P1 [Fig. 2(b)]	5×4					7.8 %
P2 [Fig. 2(d)]		5×5				7.8 %
P3 [Fig. 2(f)]	2×4	2×5				9.4%
P4 [Fig. 2(h)]	1×4	1×4	1×4	1×4	1×4	7.8 %

Table 2: Resonator dimensions and number per configuration. The mass ratio represents the resonator mass over the mass sum of the host structure and the cardboard sheet.

2.4. Experimental results

The TL measurements are presented in Fig. 3. The configurations with resonators (red solid line) are compared to the bare plate with only the spacers (blue dashed line). The artifact at 857 Hz is due to the cut-off frequency of the duct. Results are given above this frequency for information but are not relevant for our analysis. However, we can expect that they are still valid since the experimental method allows removing the contribution of higher propagating modes [29]. Also, the symmetry of the metaporoelastic structure avoids the transfer from the first to the second acoustic mode of the duct.

In all the curves, the TL first decreases (stiffness controlled zone) until the first resonance of the plate is reached and then increases roughly by 6 dB/octave, which is in line with the mass law (see the slope drawn in Fig. 3(b)). The TL at 100 Hz is related to the panel global stiffness and depends on the plate, the spacers and the mounting conditions. It varies from 15 dB to 17 dB between the configurations, which attests to good control of the boundary conditions. The lower value is obtained for configuration P1, and as a consequence, the frequency of the dip is also the lowest, i.e., 250 Hz. In addition, the dip for configuration P2, having the highest TL at 100 Hz, is reached at 295 Hz. For each configuration P_i, adding the resonators does not significantly affect the global stiffness, since the TL at 100 Hz varies by less than 1 dB.

The addition of the poroelastic resonators induces a clear increase of the TL in the region of the dip between 250 Hz and 350 Hz. As for a tuned mass damper [34, 35], when tuned on the panel first mode, the resonators almost cancel the motion of the host structure at this frequency. However, two new coupled modes appear around the tuning frequency, leading to new less significant dips because of damping. Note that for configuration P1, two peaks close to 250 Hz can be observed, which we attribute to a slight dispersion of beam properties.

Reducing the beam length from 41.5 mm (P1) to 32 mm (P2) shifts the peak from 270 Hz to 300 Hz. The value of the improvement is between 9 dB (P1) and 12 dB (P2). By covering the second face of the bare plate, an additional 3 dB is obtained. The effect of the mass ratio between the host structure and the resonator is well known [21], and covering both sides allows doubling it. The higher amplitude of the peak for the configuration P2, when compared to P1, may be explained by a better periodicity of the beam boundary conditions.

Fig. 3(c, d) shows that the use of different resonators (P3 and P4) increases the bandwidth of the metamaterial treatment. Again, covering both sides increases the effect by 2 to 3 dB.

Finally, we note that the metamaterial also affects, to a lesser extent, the region of the second mode of the bare plate, which is around 500 Hz.

3. Modeling of the finite size single panel

To further analyze the configurations tested, we model the TL of the finite size panel lined by the poroelastic resonators in the duct (Fig. 4). The geometry is the same as in configuration P1 and its parameters are listed in Tab. 3. As shown in Fig. 4 (a) and (c), the host structure's dimensions are 190 mm × 90 mm × 6 mm. We consider homogeneous properties, equivalent to the two-layer foam core cardboard used for the experiment. The host structure is clamped through an elastic surrounding layer of the same thickness whose properties are adjusted according to the first experimental resonance frequency.

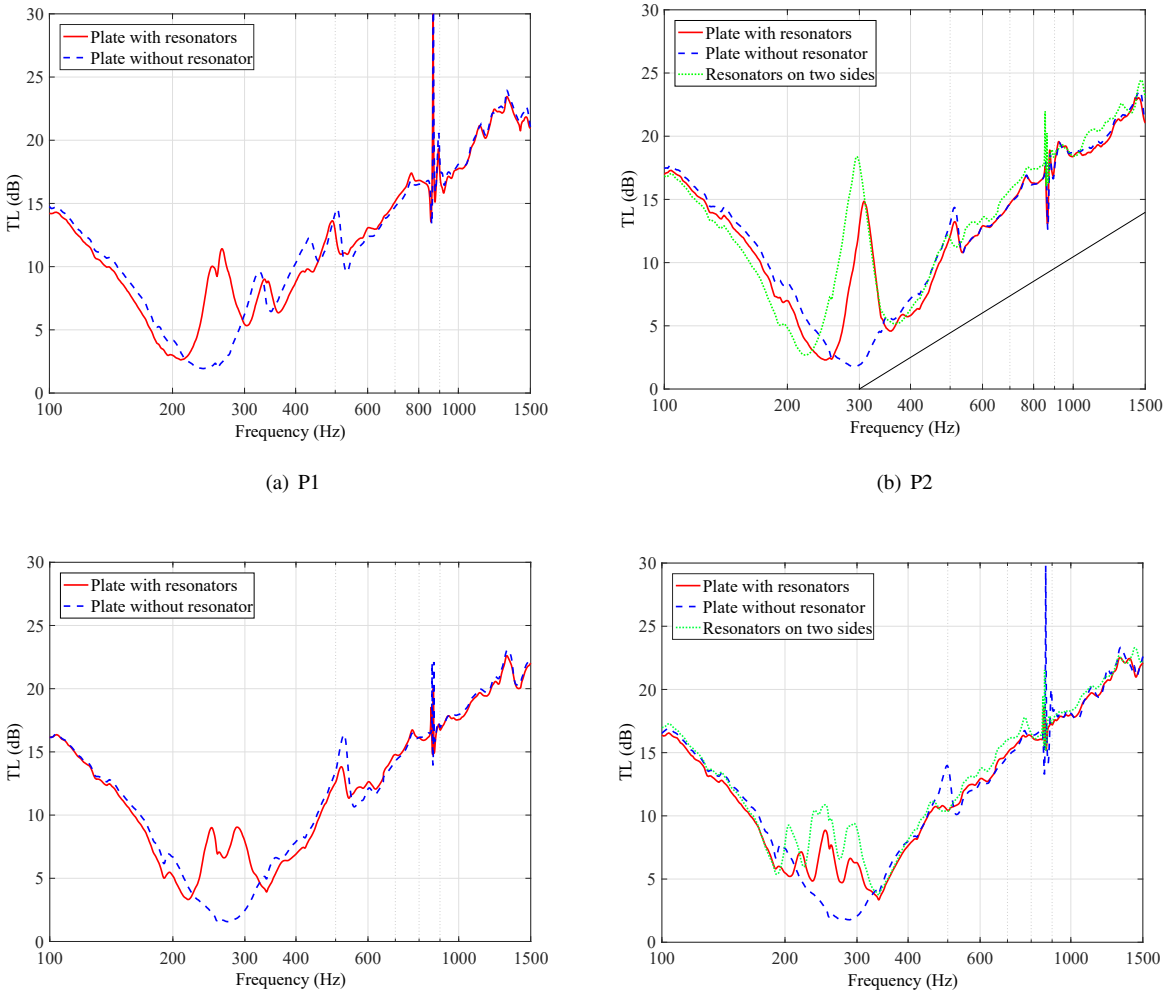

(a) P1

(b) P2

(c) P3

(d) P4

Figure 3: Measured TL of the finite size panel with and without poroelastic metamaterial at normal incidence for the different configurations. The black solid line on (b) shows the mass law slope (+6 dB per octave).

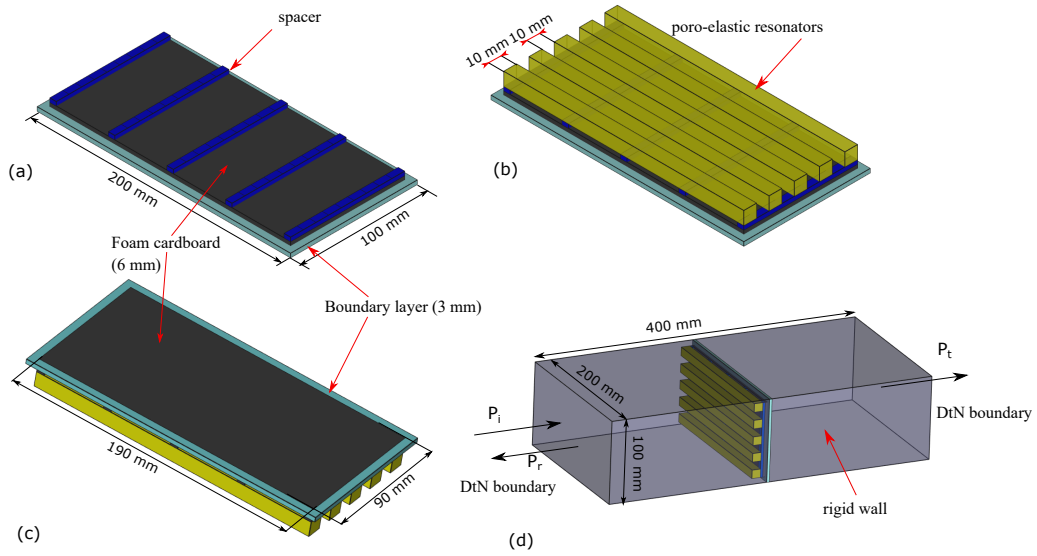

Figure 4: (a) Schematic view of the host plate, surrounding layer and spacers. (b) Structure with poroelastic resonators on spacers. (c) Rear side of the host structure. (d) Acoustic boundary conditions in the rectangular duct.

Name	Density ρ_1 kg.m^{-3}	Young's modulus E MPa	Loss factor η -	Poisson ratio ν -
Foam core cardboard	143	180	0.075	0.33
Boundary layer	800	2.0	0.075	0.20

Table 3: Homogeneous properties of the foam core cardboard and the boundary layer.

3.1. Finite element model

The global vibroacoustic problem is solved in the frequency domain (convention $e^{-i\omega t}$) using the finite element method. In the air domain, the acoustic pressure p is governed by a Helmholtz equation. On the duct walls, the acoustic normal particle velocity vanishes. The radiation conditions at both ends of the duct and the incident pressure field have been implemented using the Dirichlet-to-Neumann (DtN) map [36], using the expansion of the pressure in terms of duct acoustic modes [28]. The transmitted and reflected sound power are derived from the modal amplitude and the TL is obtained.

In the poroleastic domain Ω_p, the classical mixed ($\mathbf{u}$, p_p) formulation (see Appendix) is used with the Johnson-Champoux-Allard model. All the foam parameters are given in Tab. 1. At the interface between the fluid and the poroelastic material, the coupling conditions impose the continuity of normal displacement, pressure and normal stress (see for instance [37, Chap. 13]). In the plate, linear 3D elasticity is employed and viscoelastic losses are accounted for through a complex Young's modulus. Since the plate is clamped on the internal surface of the duct, all the displacement components vanish on that boundary. The continuity of displacement and of normal stress are imposed on the interface between elastic and air domains and the poroelastic domain. Note that the pressure and solid displacements are discretized using quadratic tetrahedral Lagrange finite elements. In all cases, the mesh size was chosen to ensure a good trade-off between accuracy and computation time.

3.2. Numerical results

Fig. 5(a) presents the TL under normal incidence of the structure with and without resonators. The first resonance frequency of the bare plate is around 254 Hz and the second one is around 400 Hz. Adding resonators shows a strong improvement of 8 dB around the first dip, due to the excitation of the first bending resonance of poroelastic beams.

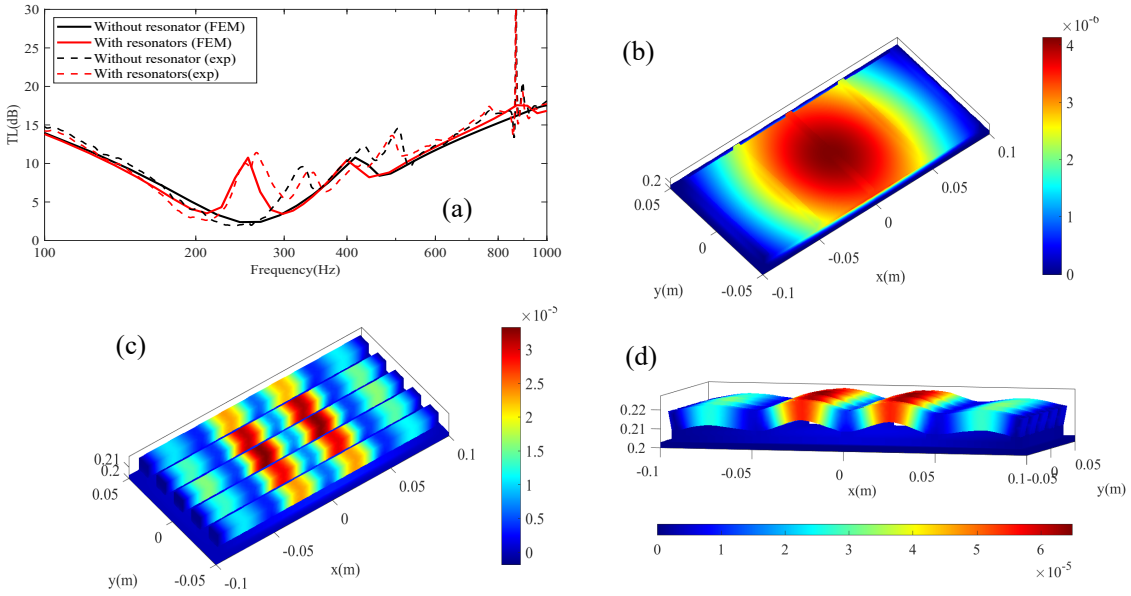

Figure 5: (a) Predicted TL of the plate with and without poroelastic resonators. (b) Displacement amplitude at 254 Hz of the bare plate (c) and of the plate with resonators. (d) Deformed mesh of resonators and plate at 254 Hz.

The numerical results are in good agreement with the experimental results of configuration P1. As observed in Fig. 5(c, d), the displacement of the beams at this frequency is higher at the center of the plate, following the first mode shape of the bare plate (see the mode shape in Fig. 5(b). The displacement of the resonators is around 10 times higher than that of the plate. As the plate is nearly motionless as this frequency, the TL is strongly improved.

3.3. Power balance

The balance between transmitted, reflected, and dissipated powers versus frequency are shown for the bare structure in Fig. 6(a) and with resonators in Fig. 6(b). The reflected and transmitted powers are calculated through modal decomposition on the duct ends [38], while the total dissipated power is deduced from energy conservation. At low frequency, the incident sound is mainly reflected. The reflection decreases until the region of the first mode (1,1) of the bare plate. At this frequency, the dynamic stiffness of the plate tends to zero and the amplitude of the plate displacement strongly increases. Most of the incident power is transmitted but limited by viscoelastic losses. At higher frequency similar trends can be observed, but the second TL dip is less pronounced because of weaker coupling with the incident field. At higher frequencies, the reflected power increases again due to the inertia effect.

When the metamaterial is added, the resonators mitigate the plate displacement at 254 Hz, which reflects back most of the incident power. The global losses are also increased, and their distribution is given in Fig. 7(a). It is seen that the dissipation within the resonators is dominant at the beam resonances. The distribution of the dissipated power within the poroelastic resonators, in terms of viscous, thermal and structural, i.e., viscoelastic dissipation [39, 40], is presented in Fig. 7(b). It is seen that structural dissipation dominates close to the beam resonances and viscous dissipation follows to a lesser extent. Thermal dissipation increases slowly over the whole frequency range.

4. Application to the infinite double panel

This section addresses the infinite double panel to focus on the dip in sound transmission loss at the mass-spring-mass resonance, above which decoupling of the two panels occurs. The assumption of infinite dimension makes sense when the lateral dimension of the double panel is much larger than its thickness: the first resonance of the finite size panel is rejected at lower frequencies and infinite plate behavior is recovered at high modal density. After recalling the features of the infinite double panel transmission loss, we present the numerical model accounting for the periodicity of the poroelastic metamaterial and the influence of the design parameters.

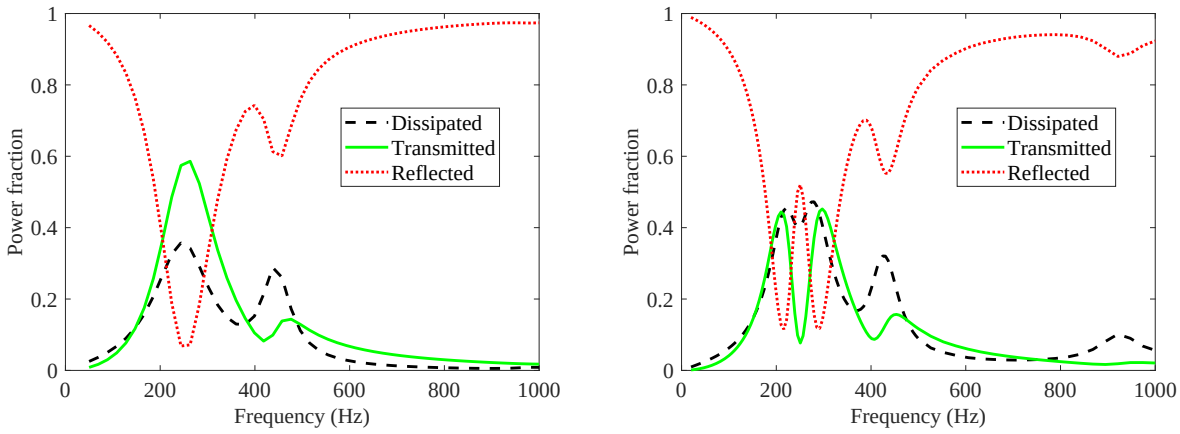

Figure 6: Fraction of three different sound powers: reflected (red dotted line), transmitted (green solid line) and dissipated (black dotted line); (a): bare structure; (b): structure with resonators.

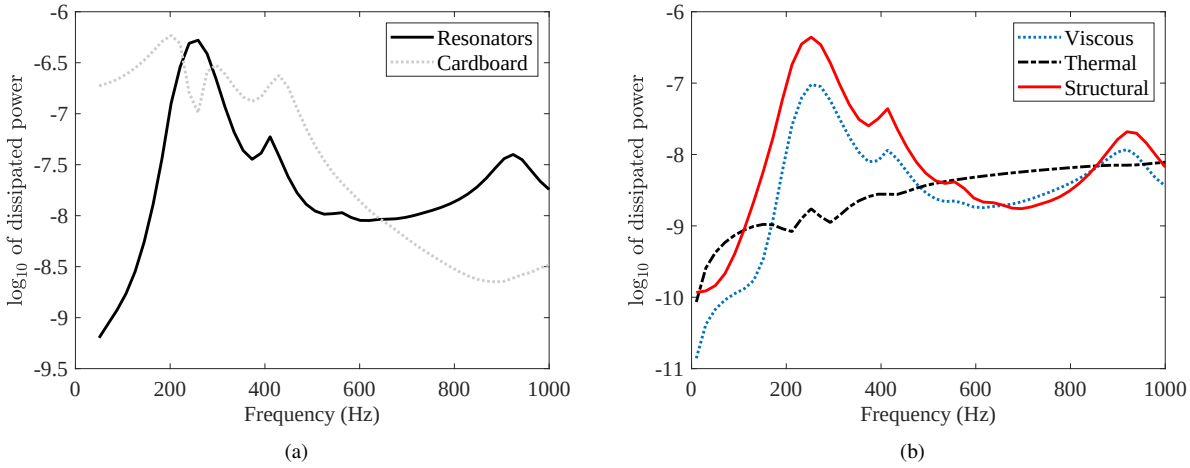

Figure 7: (a) Dissipated power in poroelastic and viscoelastic domains; (b) Distribution of viscous (blue dotted line), thermal (black dash-dotted line) and structural (red solid line) dissipation in the poroelastic domain.

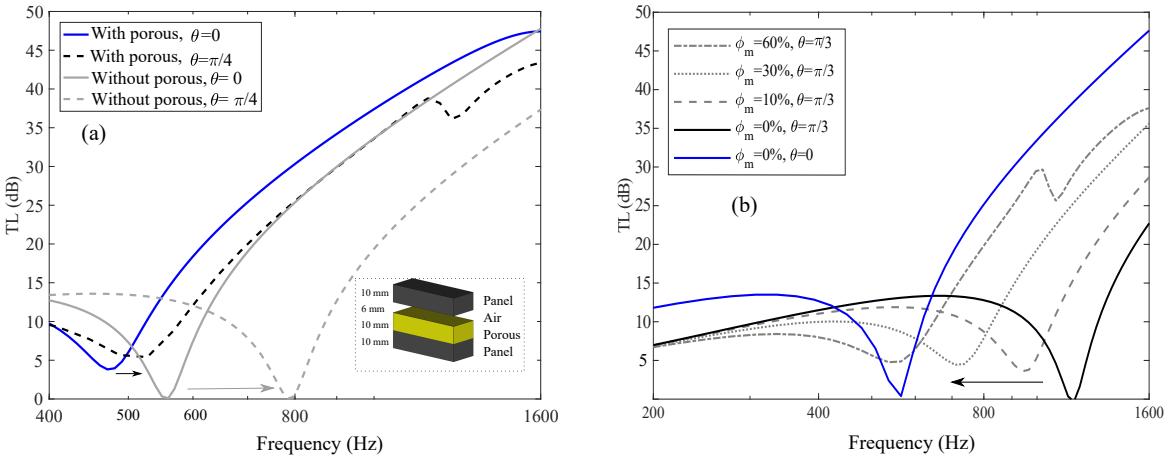

Figure 8: (a) Impact of the incidence angle on the transmission loss dip frequency of the double panel with and without porous material filling; (b) Impact of porous filling ratio ϕ_m on decoupling efficiency.

4.1. Infinite double panel filled with an homogeneous porous layer

A double panel partially filled with a homogeneous poroelastic layer is considered, as shown in Fig. 8. This configuration, simulated by the transfer matrix method (TMM) [37, Chap. 11] using Maine3A code, will be used as the validation case and as an illustration of the main features of the double panel sound transmission (see [41]). The elastic plate thickness is 10 mm. The plates are separated by 16 mm. The porous layer nominal thickness is $H = 10$ mm. The properties of both media are given in Tab. 1 and 3.

Fig. 8(a) illustrates the effect of the incidence angle and cavity filling. The decoupling frequency at normal incidence without porous material is observed around 550 Hz. This frequency can be estimated by [1, Eq. (5.75)]

$$f_r = \frac{1}{2\pi}\sqrt{\frac{K}{h\,\cos^2\theta}\,\frac{m_1+m_2}{m_1 m_2}}, \tag{2}$$

where K is the bulk modulus of the fluid layer of thickness h, θ is the incidence angle ($\theta = 0$ corresponds to normal incidence), m_1 and m_2 are the surface densities of each panel. In the adiabatic regime, $K = \gamma P_0$, where P_0 denotes the atmospheric pressure and $\gamma = 1.4$ is the ratio of specific heats. This decoupling frequency increases up to nearly 800 Hz for an incidence angle of $\pi/4$.

When filling the cavity with the porous material, the decoupling frequency at normal incidence decreases below 500 Hz. Indeed, the presence of porous material lowers the bulk modulus of the air from its adiabatic to isothermal value, from γP_0 to P_0, respectively. Thermal losses will also damp the resonance and attenuate the dip. Furthermore, the decoupling frequency remains close to 500 Hz for an incidence angle of $\pi/4$. This can be attributed to the smaller sound velocity in the porous material c_e compared to c_0 in the air [37]. According to the Snell-Descartes law, $\sin\theta_e = c_e/c_0 \sin\theta$, the incident angle θ_e in the porous layer is less than that in the air. For instance, at a frequency of 470 Hz, the ratio of the sound velocity in the porous material over that in the air is around 0.25, which indicates the θ_e is 12.5° for $\theta = 60°$. This will minimize the impact of the incidence angle. Fig. 8(b) shows that this effect increases with the filling fraction of the cavity, here increasing from 0% to 60% for an incident angle of $\pi/3$: the decoupling frequency becomes independent of the incidence angle from the porous filling fraction of 60%. This feature contributes to achieving efficient decoupling for a diffuse field excitation, representing an advantage of the metaporoelastic structure. In this way, the finite size of the cavity limits the sensitivity of the decoupling frequency to the incidence angle [42]. Finally, the presence of the porous material mitigates the acoustic resonances between the two panels.

4.2. Periodic finite element model

The finite element model takes advantage of the periodicity of the poroelastic metamaterial since wave propagation in an infinite periodic media excited by a plane wave can be handled by using the Floquet-Bloch theorem to reduce computation time. We use the same approach as in our previous work [27], where only a unit cell with pseudo-periodic boundary conditions on all lateral sides is considered, as shown in Fig. 9(a). Lattice vector $\mathbf{l}$ is $\left(l_x, l_y, 0\right)$. In the unit cell, the fluid, poroelastic, and the elastic domains are discretized using quadratic Lagrange tetrahedral finite elements, as before.

Incident plane wave P_I impinges on the top surface of the air domain with the wavevector

$$\mathbf{k} = -k_a \left(\sin\theta \cdot \cos\varphi, \sin\theta \cdot \sin\varphi, \cos\theta\right), \tag{3}$$

where θ is the inclination and φ is the azimuth (see Fig. 9(a)). The homogeneous plates are independent of φ, but because of the orientation of the resonators, the lined panel presents slight anisotropy at low frequency.

The radiation condition of the scattered field in the top and bottom air domain is implemented with a 'Dirichlet to Neumann' map based on Floquet mode decomposition [27]. The amplitude of the reflected power and the power of transmitted wave P_T can be recovered by projection on the Floquet-Bloch modes. The transmission coefficient at a specific angle is $\tau(\theta, \varphi) = P_T(\theta, \varphi)/P_I(\theta, \varphi)$. Under a diffuse field, the transmission coefficient τ_d is obtained by integrating τ over the incident angles as in the following:

$$\tau_d = \frac{1}{\pi} \frac{\int_0^{\pi} \int_0^{\theta_{lim}} \tau(\theta, \varphi) \sin\theta \cos\theta \, \mathrm{d}\theta \, \mathrm{d}\varphi}{\int_0^{\theta_{lim}} \sin\theta \cos\theta \, \mathrm{d}\theta}. \tag{4}$$

Here, $\theta_{lim} = 78°$ for the diffuse field transmission, as in Ref. [37].

4.3. Numerical results

Firstly, let us consider the effect of the proposed poroelastic metamaterial at normal incidence. The distance between the two panels is 16 mm to obtain a porous filling fraction of 42%, as shown in Fig. 9(a). It is recalled that poroelastic beams are separated from each other by a 5 mm air gap. To keep the mass-spring-mass frequency around 300 Hz, the plate surface density is set to 4 kg.m^{-2}. The porous density is set to 96.8 kg.m^{-3} to obtain a mass ratio of 8%. The Young's modulus of the porous material is tuned to 97 kPa to match the double panel resonance.

Fig. 9(b) shows the TL at normal incidence for a poroelastic metamaterial to total structure mass ratio between 2% and 8%. To maintain the same beam resonance frequency, the density and Young's modulus of the poroelastic material are modified together. It is shown that the amplitude of TL enhancement increases from 12 dB to 25 dB in the region of the mass-spring-mass dip around $f = 300$ Hz, which is in line with previous works [14]. In comparison with the homogeneous layer having the same volume as the poroelastic resonators (equivalent thickness of 6.6 mm) and separated by the same distance from the plate (3 mm), the 2% configuration increases the minimal TL from 3 dB to 8 dB.

4.4. Power balance

Fig. 10 compares the fraction distribution of the dissipated, transmitted, and reflected sound powers for the bare and treated double panel with an added mass ratio of 8%. For the bare double panel, the sound power is almost perfectly reflected except around $f = 300$ Hz, corresponding to the TL dip occurring at the decoupling frequency f_r. Due to the resonance, the sound power is almost perfectly transmitted. When the resonators are added to the first panel, the transmitted power is drastically reduced. The TL peak does not correspond to a dissipation peak but to the strong reflection of the incident wave on the motionless first panel, as stated in section 3.2. The effect of the two reflected power dips are counterbalanced by the dissipation within the poroelastic resonators.

The dissipated power in both domains, i.e., panels and poroelastic resonators, is shown in Fig. 11(a). The highest mitigated power in both domains corresponds to the first TL dip. Most of the dissipation occurs within the poroelastic resonators since the panels have a nearly rigid body motion in this regime. Fig. 11(b) presents the distribution of the dissipated power within the poroelastic resonators. The three dissipation components are also maximal around the decoupling frequency and the structural one dominates in this region. Unlike the finite size single panel (see Fig. 6), the thermal dissipation is also maximal in this region, since the pressure amplitude in the cavity between the two panels is maximal at the mass-spring-mass resonance.

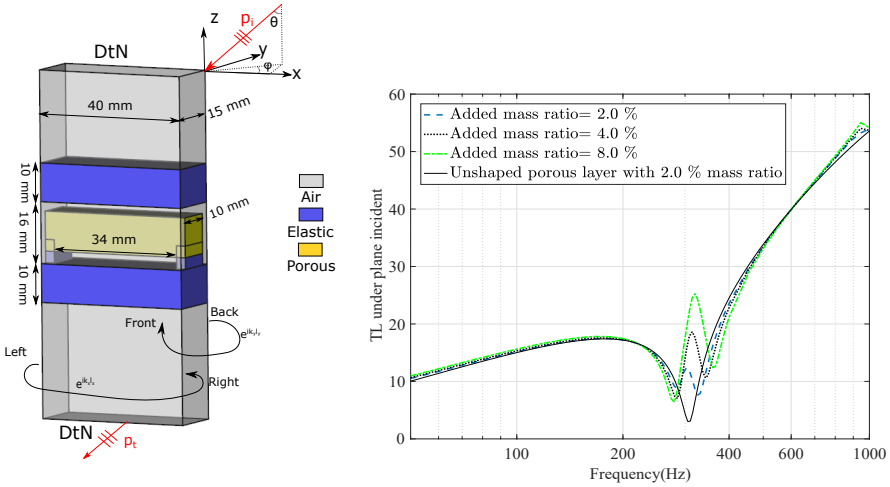

(a) (b)

Figure 9: Double panel with poroelastic resonators: (a) periodic cell geometry and (b) results for the nominal configuration for the bare, porous lining and poroelastic metamaterial at normal incidence.

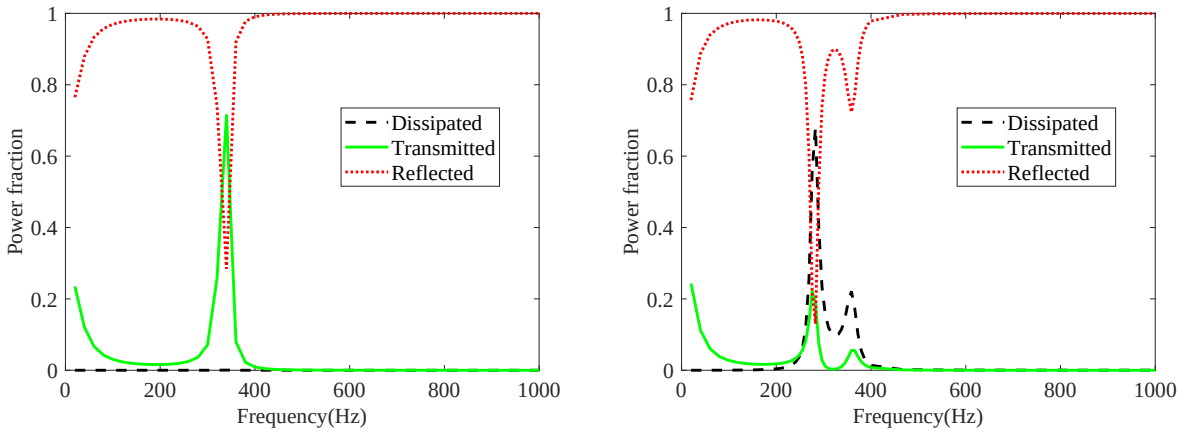

(a) (b)

Figure 10: Dissipated (black dashed line), transmitted (green solid line) and reflected (red dotted line) power with respect to the frequency. (a) bare structure; (b) structure with resonators.

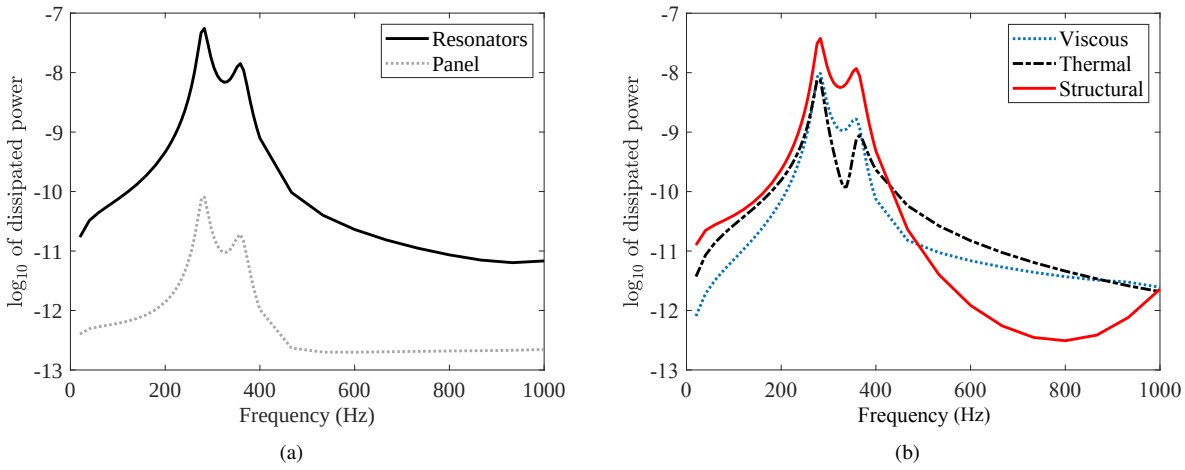

Figure 11: (a) Distribution of dissipated power in poroelastic and viscoelastic domains; (b) Distribution of viscous (blue dotted line), thermal (black dash-dotted line) and structural (red solid line) dissipation in the poroelastic domain.

4.5. Parametric analysis

This section addresses the influence of several parameters of the poroelastic resonators on the transmission loss in the diffuse field. Fig. 12(a-b) presents the influence of the airflow resistivity. This parameter accounts for viscous stresses and controls the losses and the coupling between the fluid and the solid phase. At high frequencies, above the decoupling frequency, increasing the airflow resistivity improves the TL by absorbing the residual acoustic waves that are not reflected back by the panel decoupling, as shown in Fig. 12(a). However, beyond a specific value, here above σ^* ($*$ exponent stands for nominal values), the TL decreases at high frequencies, approaching the limit of the non-porous material, as shown in Fig. 12(b). In this case, acoustic waves are no longer dissipated by the porous material and the decoupling tends to occur at higher frequencies because the apparent air volume in the cavity is reduced.

In the vicinity of the poroelastic metamaterial resonance, the airflow resistivity acts conversely. The two TL dips around this resonance are less pronounced for smaller airflow resistivities, the worst case being the nominal resistivity σ^*. This is related to the damping of the resonators, which depends on the relative motion between the solid and fluid phases and of the viscous stresses. For a small airflow resistivity, the relative motion is maximal, whereas the viscous stresses are maximal for a high airflow resistivity. The optimal airflow resistivity depends on the airgap size, beam dimensions, and resonance frequency of the double panel. The effect of the resonator skeleton loss factor is also illustrated in Fig. 12(c) at normal incidence, by varying it from its nominal value η^* up to 10 times this value. It can be seen that damping reduces the side dips and TL peak since beyond a given damping the metamaterial no longer resonates.

Finally, Fig. 12(d) shows that by controlling its thickness, reducing the volume of the poroelastic metamaterial in the cavity alters the efficiency of the decoupling as observed for the homogeneous layer presented in Fig. 8. However, the TL enhancement around the decoupling frequency, already observed in normal incidence, is robust and kept significant for the diffuse field excitation.

5. Conclusion

In this study, a poroelastic metamaterial is proposed to improve the acoustic insulation performance of a finite size single panel and an infinite double panel in the region of their first dip. The metamaterial is composed of a set of periodic poroelastic beams the first bending mode of which is tuned according to the mode of the host structure addressed. The concept was illustrated experimentally using thermocompressed melamine foam, giving a suitable balance between the quality factor of the beam resonance and dissipation. A gain up to 12 dB was achieved

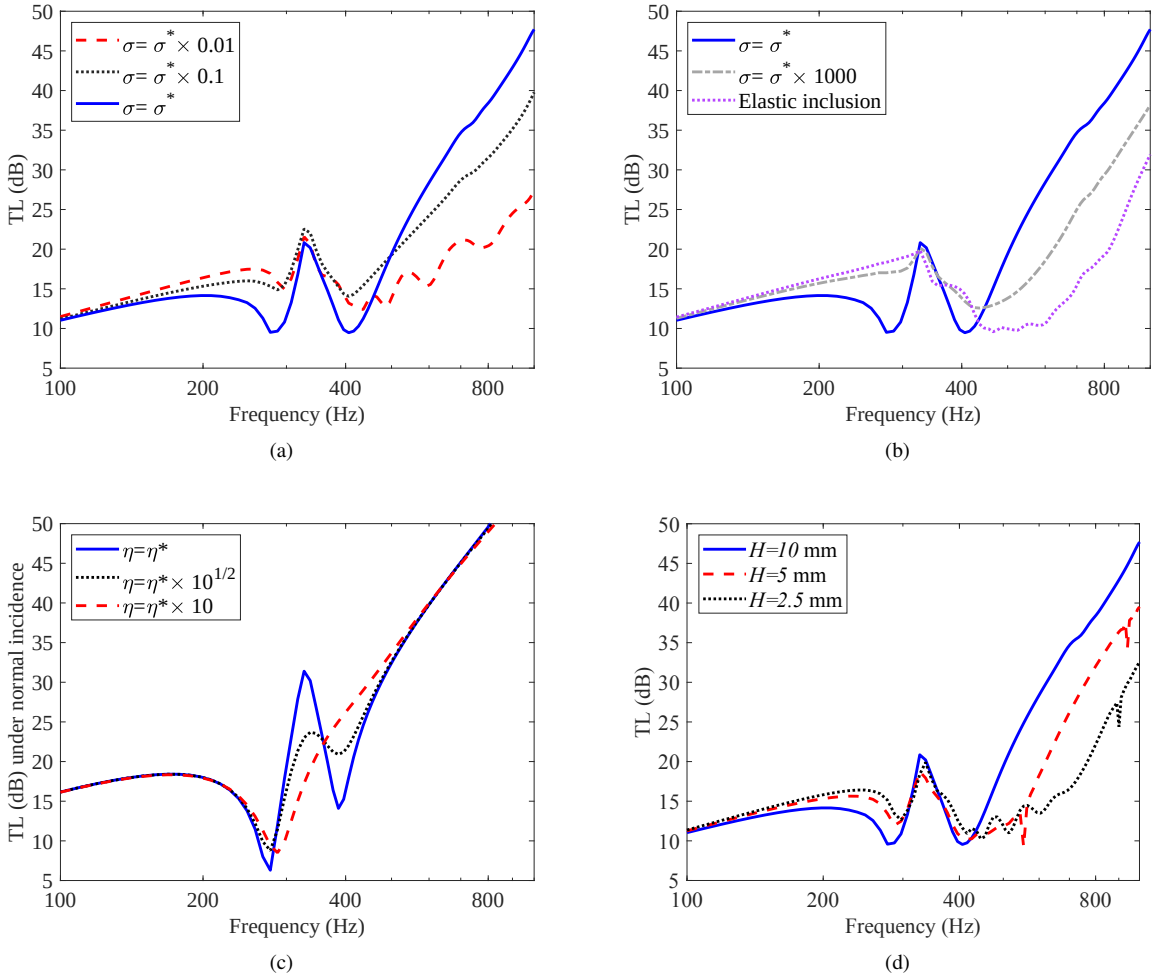

Figure 12: The transmission loss (TL) in the diffuse field of the double panel with different airflow resistivities of (a) $\sigma = \sigma^* \times (0.01, 0.1, 1)$, (b) $\sigma = \sigma^* \times (1, 1000)$ and elastic inclusion, (c) TL under normal incidence of the double panel with resonators with different loss factors, (d) TL in the diffuse field of the double panel with a resonator filling fraction of ϕ_m =0.4, 0.2 and 0.1.

experimentally and could be spread out with multiple resonators. A numerical analysis using a finite element model was performed and confirmed the experimental observations. It showed that structural dissipation was dominant in the region of the metamaterial resonances, followed by viscous dissipation, and by thermal dissipation only in the double panel partition.

For the double wall application, the numerical analysis was performed assuming a periodic resonator arrangement. It showed that the decoupling frequency was almost independent of the incidence angle for a porous filling fraction greater than 60%. Moreover, the airflow resistivity allowed controlling both the side dips and the transmission loss at higher frequencies.

This poroelastic metamaterial provided an integrated means of combining the properties of the sound absorbing material and vibration control. The next step is to design and optimize this concept on real double panels for building and automotive applications.

Acknowledgements

This work was partially funded by the China Scholarship Council (No.201701810142). The authors would like to thank Thomas Boutin for sample manufacturing and Yorick Buot de l'Epine for the experimental setup.

Appendix: Mixed ($\mathbf{u}$, p_p) formulation

In the poroelastic domain, the acoustic fields are described by the ($\mathbf{u}$, p_p) formulation of the Biot model [37, Chap. 13],

$$\nabla \cdot \boldsymbol{\sigma}^s(\mathbf{u}) + \omega^2 \rho\, \mathbf{u} + \gamma\, \nabla p_p = 0, \tag{5a}$$

$$\Delta p_p + \omega^2 \frac{\rho_{22}}{R} p_p - \omega^2 \frac{\rho_{22}}{\phi^2} \gamma\, \nabla \cdot \mathbf{u} = 0. \tag{5b}$$

Here, p_p is the pore pressure, ϕ is the porosity of the porous material, $\gamma = \phi\left(\frac{\rho_{12}}{\rho_{22}} - \frac{Q}{R}\right)$ and $\rho = \rho_{11} - \frac{\rho_{12}^2}{\rho_{22}}$. Coefficient R is the effective bulk modulus of the fluid phase and takes into account the thermal dissipation, Q couples the two phases by volume dilatation. The effective density coefficient ρ_{11} and ρ_{22}, for the solid phase and the fluid phase, respectively, and the coupling density coefficient ρ_{12} are complex-valued, and their imaginary part takes into account viscous losses. The first two terms in (5a) and in (5b) describe the dynamics of the elastic skeleton and equivalent fluid respectively. The last term in both equations couples the two phases. The *in vacuo* stress tensor $\boldsymbol{\sigma}^s$ is given by

$$\boldsymbol{\sigma}(\mathbf{u}) = \mathbf{I}\left(K_b - \frac{2}{3}N\right)\nabla \cdot \mathbf{u} + 2N\boldsymbol{\varepsilon}^s(\mathbf{u}). \tag{6}$$

Here, K_b is the complex dynamic bulk modulus of the frame, N is the shear modulus. Both include the structural damping.

In the plate, the acoustic perturbation of the displacement $\mathbf{u}$ fulfil the three dimensional elasto-dynamic equations,

$$\nabla \cdot \boldsymbol{\sigma}^s(\mathbf{u}) + \omega^2 \rho\, \mathbf{u} = 0, \tag{7}$$

with the standard Hooke stress-strain relations,

$$\boldsymbol{\sigma}(\mathbf{u}) = \lambda \mathbf{I} \nabla \cdot \mathbf{u} + 2\mu\boldsymbol{\varepsilon}^s(\mathbf{u}), \tag{8}$$

where quantities λ and μ are the Lamé coefficients.

References

[1] F. Fahy, P. Gardonio, Sound and structural vibration: radiation, transmission and response: second edition, Academic Press, 2007.

[2] S. J. Estéve, M. E. Johnson, Reduction of sound transmission into a circular cylindrical shell using distributed vibration absorbers and helmholtz resonators, The Journal of the Acoustical Society of America 112 (6) (2002) 2840–2848. doi:10.1121/1.1514933.

[3] C. Droz, O. Robin, M. Ichchou, N. Atalla, Improving sound transmission loss at ring frequency of a curved panel using tunable 3D-printed small-scale resonators, The Journal of the Acoustical Society of America 145 (2019) 72. doi:10.1121/1.5088036.

[4] M. Strasberg, D. Feit, Vibration damping of large structures induced by attached small resonant structures, The Journal of the Acoustical Society of America 99 (1) (1996) 335–344. doi:10.1121/1.414545.

[5] J. Mason, F. Fahy, The use of acoustically tuned resonators to improve the sound transmission loss of double-panel partitions, Journal of Sound and Vibration 124 (2) (1988) 367–379. doi:10.1016/S0022-460X(88)80194-9.

[6] P. Sheng, X. Zhang, Z. Liu, C. T. Chan, Locally resonant sonic materials, Physica B: Condensed Matter 338 (1-4) (2003) 201–205. doi:10.1016/s0921-4526(03)00487-3.

[7] S. H. Lee, C. M. Park, Y. M. Seo, Z. G. Wang, C. K. Kim, Acoustic metamaterial with negative density, Physics letters A 373 (48) (2009) 4464–4469. doi:10.1016/j.physleta.2009.10.013.

[8] M. Sigalas, E. Economou, Elastic waves in plates with periodically placed inclusions, Journal of Applied Physics 75 (6) (1994) 2845–2850. doi:10.1063/1.356177.

[9] D. Yu, Y. Liu, G. Wang, H. Zhao, J. Qiu, Flexural vibration band gaps in timoshenko beams with locally resonant structures, Journal of applied physics 100 (12) (2006) 124901. doi:10.1063/1.2400803.

[10] Y. Pennec, B. Djafari Rouhani, H. Larabi, A. Akjouj, J. N. Gillet, J. O. Vasseur, G. Thabet, Phonon transport and waveguiding in a phononic crystal made up of cylindrical dots on a thin homogeneous plate, Phys. Rev. B 80 (2009) 144302. doi:10.1103/PhysRevB.80.144302.

[11] Y. Xiao, J. Wen, X. Wen, Flexural wave band gaps in locally resonant thin plates with periodically attached spring–mass resonators, Journal of Physics D: Applied Physics 45 (19) (2012) 195401. doi:10.1088/0022-3727/45/19/195401.
[12] J.-P. Groby, C. Lagarrigue, B. Brouard, O. Dazel, V. Tournat, B. Nennig, Enhancing the absorption properties of acoustic porous plates by periodically embedding helmholtz resonators, The Journal of the Acoustical Society of America 137 (1) (2015) 273–280. doi:10.1121/1.4904534.
[13] M. Yang, P. Sheng, Sound absorption structures: From porous media to acoustic metamaterials, Annual Review of Materials Research 47 (2017) 83–114. doi:10.1146/annurev-matsci-070616-124032.
[14] Z. Liu, R. Rumpler, L. Feng, Broadband locally resonant metamaterial sandwich plate for improved noise insulation in the coincidence region, Composite Structures 200 (2018) 165–172. doi:10.1016/j.compstruct.2018.05.033.
[15] Y. Song, J. Wen, H. Tian, X. Lu, Z. Li, L. Feng, Vibration and sound properties of metamaterial sandwich panels with periodically attached resonators: Simulation and experiment study, Journal of Sound and Vibration 489 (2020) 115644. doi:10.1016/j.jsv.2020.115644.
[16] S. Sugie, J. Yoshimura, T. Iwase, Effect of inserting a Helmholtz resonator on sound insulation in a double-leaf partition cavity, Acoustical Science and Technology 30 (5) (2009) 317–326. doi:10.1250/ast.30.317.
[17] F. Langfeldt, H. Hoppen, W. Gleine, Broadband low-frequency sound transmission loss improvement of double walls with Helmholtz resonators, Journal of Sound and Vibration 476 (2020) 115309. doi:10.1016/j.jsv.2020.115309.
[18] N. G. de Melo Filho, L. Van Belle, C. Claeys, E. Deckers, W. Desmet, Dynamic mass based sound transmission loss prediction of vibro-acoustic metamaterial double panels applied to the mass-air-mass resonance, Journal of Sound and Vibration 442 (2019) 28–44. doi:10.1016/j.jsv.2018.10.047.
[19] M. R. Kidner, C. R. Fuller, B. Gardner, Increase in transmission loss of single panels by addition of mass inclusions to a poro-elastic layer: Experimental investigation, Journal of Sound and Vibration 294 (3) (2006) 466–472. doi:10.1016/j.jsv.2005.11.022.
[20] N. de Melo Filho, C. Claeys, E. Deckers, W. Desmet, Metamaterial foam core sandwich panel designed to attenuate the mass-spring-mass resonance sound transmission loss dip, Mechanical Systems and Signal Processing 139 (2020) 106624. doi:10.1016/j.ymssp.2020.106624.
[21] J. Li, S. Li, Sound transmission through metamaterial-based double-panel structures with poroelastic cores, Acta Acustica united with Acustica 103 (5) (2017) 869–884. doi:10.3813/aaa.919114.
[22] Y. Xiao, J. Wen, X. Wen, Sound transmission loss of metamaterial-based thin plates with multiple subwavelength arrays of attached resonators, Journal of Sound and Vibration 331 (25) (2012) 5408–5423. doi:10.1016/j.jsv.2012.07.016.
[23] J. Legault, N. Atalla, Numerical and experimental investigation of the effect of structural links on the sound transmission of a lightweight double panel structure, Journal of Sound and Vibration 324 (3-5) (2009) 712–732. doi:10.1016/j.jsv.2009.02.019.
[24] Y. Xiao, J. Wen, L. Huang, X. Wen, Analysis and experimental realization of locally resonant phononic plates carrying a periodic array of beam-like resonators, Journal of Physics D: Applied Physics 47 (4) (2013) 045307. doi:10.1088/0022-3727/47/4/045307.
[25] X.-F. Lv, K.-C. Chuang, A. Erturk, Tunable elastic metamaterials using rotatable coupled dual-beam resonators, Journal of Applied Physics 126 (3) (2019) 035107. doi:10.1063/1.5099324.
[26] J. Christensen, V. Romero-García, R. Picó, A. Cebrecos, F. G. De Abajo, N. A. Mortensen, M. Willatzen, V. J. Sánchez-Morcillo, Extraordinary absorption of sound in porous lamella-crystals, Scientific reports 4 (1) (2014) 1–5. doi:10.1038/srep04674.
[27] N. Dauchez, B. Nennig, O. Robin, Additional sound absorption within a poroelastic lamella network under oblique incidence, Acta Acust. United Ac 104 (2) (2018) 211–219. doi:10.3813/aaa.919162.
[28] K. Li, B. Nennig, E. Perrey-Debain, N. Dauchez, Poroelastic lamellar metamaterial for sound attenuation in a rectangular duct, Applied Acoustics 176 (2021) 107862. doi:10.1016/j.apacoust.2020.107862.
[29] H. Trabelsi, N. Zerbib, J. M. Ville, F. Foucart, Passive and active acoustic properties of a diaphragm at low Mach number, Experimental procedure and numerical simulation, European Journal of Computational Mechanics 20 (1-4) (2011) 49–71. doi:10.3166/EJCM.20.49-71.
[30] R. D. Blevins, Formulas for dynamics, acoustics and vibration, John Wiley & Sons, 2015.
[31] L. Lei, N. Dauchez, J. D. Chazot, Generalized power law for predicting the air flow resistivity of thermocompressed fibrous materials and open cell foams, Applied Acoustics 143 (2019) 59–65. doi:10.1016/j.apacoust.2018.08.029.
[32] L. Lei, N. Dauchez, J. D. Chazot, Prediction of the six parameters of an equivalent fluid model for thermocompressed glass wools and melamine foam, Applied Acoustics 139 (2018) 44–56. doi:10.1016/j.apacoust.2018.04.010.
[33] N. Dauchez, M. Etchessahar, S. Sahraoui, On measurement of mechanical properties of sound absorbing materials, in: Poromechanics II, CRC Press, 2020, pp. 627–631.
[34] D. J. Mead, Passive vibration control, John Wiley & Sons, 1998.
[35] M. D. Martínez-Rodrigo, P. Museros, Optimal design of passive viscous dampers for controlling the resonant response of orthotropic plates under high-speed moving loads, Journal of Sound and Vibration 330 (7) (2011) 1328–1351.
[36] I. Harari, I. Patlashenko, D. Givoli, Dirichlet-to-neumann maps for unbounded wave guides, J. Comp. Phys. 143 (1) (1998) 200 – 223. doi:10.1006/jcph.1998.5960.
[37] J.-F. Allard, N. Atalla, Propagation of Sound in Porous Media: Modelling Sound Absorbing Materials, John Wiley and Sons, 2009. doi:10.1002/9780470747339.
[38] R. Binois, E. Perrey-Debain, N. Dauchez, B. Nennig, J.-M. Ville, G. Beillard, On the efficiency of parallel baffle-type silencers in rectangular ducts: Prediction and measurement, Acta Acustica united with Acustica 101 (3) (2015) 520–530. doi:10.3813/aaa.918849.
[39] O. Dazel, F. Sgard, F.-X. Becot, N. Atalla, Expressions of dissipated powers and stored energies in poroelastic media modeled by {u, U} and {u, P} formulations, The Journal of the Acoustical Society of America 123 (4) (2008) 2054–2063. doi:10.1121/1.2874520.
[40] O. Doutres, N. Dauchez, J.-M. Génevaux, Porous layer impedance applied to a moving wall: Application to the radiation of a covered piston, The Journal of the Acoustical Society of America 121 (1) (2007) 206–213. doi:10.1121/1.2359233.
[41] T. Shimizu, M. Toyoda, D. Takahashi, Y. Kawai, Numerical analysis of the influence of acoustic resonance in air cavities between window-panes on sound transmission loss, Applied Acoustics 74 (8) (2013) 1010–1017. doi:10.1016/j.apacoust.2012.12.005.
[42] J. E. Cambridge, J. L. Davy, J. Pearse, The influence of finite and infinite wall cavities on the sound insulation of double-leaf walls, The Journal

of the Acoustical Society of America 141 (1) (2017) 207–218, publisher: Acoustical Society of America. doi:10.1121/1.4973570.
URL https://asa.scitation.org/doi/10.1121/1.4973570